Multimodal investigation of a keloid scar by combining mechanical tests *in vivo* with diverse imaging techniques

Jérôme Chambert[a,b,*], Thomas Lihoreau[c], Sylvain Joly[a,b], Brice Chatelain[d], Patrick Sandoz[a,b], Philippe Humbert[e], Emmanuelle Jacquet[a,b], Gwenaël Rolin[c,e]

[a] *FEMTO-ST Institute, Univ. Bourgogne Franche-Comté, CNRS*
[b] *Department of Applied Mechanics, 24 rue de l'Épitaphe, 25000 Besançon, France*
[c] *Centre Hospitalier Universitaire de Besançon, INSERM, CIC 1431, Centre d'Investigation Clinique, 25030 Besançon, France*
[d] *Centre Hospitalier Universitaire de Besançon, Service de chirurgie maxillo-faciale, stomatologie et odontologie hospitalière, Besançon, France*
[e] *Univ. Bourgogne Franche-Comté, INSERM, EFS BFC, UMR1098, Interactions Hôte-Greffon-Tumeur / Ingénierie Cellulaire et Génique, Besançon, France*

Abstract

Keloids are pathologic scars, defined as fibroproliferative diseases resulting from abnormal wound responses, which grow beyond the original wound margins. They develop on specific pro-keloid anatomic sites frequently characterized by high stress states. The initiation and growth mechanisms of keloid are not well-understood.

This study relates multimodal investigation of a keloid by using mechanical tests *in vivo* and imaging techniques. A single case composed of a keloid, the healthy skin surrounding the keloid, and the contralateral healthy skin on the upper arms of a woman has been investigated in extension and suction by using non-invasive devices dedicated to *in vivo* skin measurement. The thickness and microstructure of these soft tissues have been observed by echography, tomography and confocal microscopy. Displacement fields

have been obtained by using digital image correlation.

Unlike healthy skin, keloid is not a well-defined multilayer structure: the frontier between epidermis and dermis disappears. The mechanical behavior of keloid is highly different from healthy skin one. The R-parameters have been deduced from suction curves. Physical parameters as tissue extensibility, initial and final tangent moduli have been identified from the stress-strain curves. The extensibility (respectively, initial rigidity) of keloid is highly lower (respectively, higher) than that of healthy skin. To compare the final rigidity of keloid versus healthy skin, further tests have to be performed with higher strain values.
Keywords: Keloid, *In vivo* measurements, Skin mechanical behavior, Imaging, Biomechanics

1. Introduction

Keloids are pathologic scars defined as fibroproliferative diseases resulting from abnormal wound responses (Bayat et al., 2003). These dermal pseudo-tumors may occur after several skin injuries (surgery, burns, trauma, skin piercing, folliculitis, etc.), are able to grow beyond the initial site of skin injury and to persist long in time without natural regression (Butler et al., 2008). Clinically, keloids are raised, firm and hyperpigmented scars affecting young people (10 to 30 years). They occur mainly on chest, shoulders, neck and ears in patients with high phototype (Bayat et al., 2003).

*Correspondence address: Dr Jérôme Chambert, FEMTO-ST Institute, Department of Applied Mechanics, 24 rue de l'Épitaphe, 25000 Besançon, France, Tel.: +33 3 81 66 60 25; Fax: +33 3 81 66 67 00, Email: jerome.chambert@univ-fcomte.fr

Currently, treatments against keloids are multiple, sometimes empirical (Ud-Din and Bayat, 2013) and their effectiveness is relative. Some papers reported reduction in scar inflammation (Daya, 2011; Atkinson et al., 2005), or no keloid development after treatment with adhesive band positioned in order to reduce the tension exerted in the wound region post keloid surgery (Atkinson et al., 2005). Combinaison of compression therapy and silicon sheets has been tested to manage keloid scarring (Fraccalvieri et al., 2013). Huang et al. (2014) have paid attention to the histological characteristics of keloids, compared to healthy skin and hypertrophic scars in order to better discriminate them and to adapt treatment strategies. Nevertheless, there is no gold-standard to both objectivate therapeutic outcome and compare the efficacy of potential treatments.

In addition, structural differences for both epidermal and dermal layers have been described. Limandjaja et al. (2017) concluded that keloids showed increased epidermal thickness compared with healthy skin, normotrophic and hypertrophic scars. This was not due to hyperproliferation, but possibly caused by abnormal early terminal differentiation, which affects *stratum corneum* formation. They also showed that epidermis is more flattened in keloid than in safe skin. Structural and histological architecture for healthy skin and keloid scars is strongly different (Suttho et al., 2017). Novel imaging strategies have been proposed to assess the volume, the orientation, the thickness and the anatomical limits of fibrotic tissue (Reinholz et al., 2016; Salameh et al., 2018).

Past years, occurrence and evolution of keloid scars have been linked to several supposed mechanisms: cell dysfunction (Lim et al., 2001; Meenakshi et al., 2005), genetics (Marneros et al., 2004), inflammation (Ogawa, 2008),

skin mechanical properties (Ramakrishnan et al., 1974; Wang et al., 2006). However, these hypotheses do not result in a satisfactory understanding of keloid scars, in particular the mechano-structuro-biological interplay should be explored.

Indeed at a cellular level, mechanical forces are involved in all steps of skin wound healing. Their distribution changes during wounding, notably because myofibroblasts produce traction forces during matrix remodeling. Several *in vivo* and *in vitro* studies (Ogawa and Hsu, 2013; Al-Attar et al., 2006) have led to a relation between the pathogenesis of skin disorders and mechano-biological dysfunction. At macroscopic scale, mechanical properties of keloid scars are different from healthy skin. Rockwell et al. (1989) suggested first the contribution of mechanical stresses in keloid formation. Keloids occur predominantly at anatomical sites submitted to high tension forces, such as chest, neck or shoulder (Ogawa, 2008; Chike-Obi et al., 2009), and usually related to normal body movements. Similar observation has been reported by Ogawa and Orgill (2009) who proposed the relationship between abnormal scars and incisions made across skin tension lines. Other analyses lead to the same conclusion on scars (Cerda, 2005), hypertrophic scars (Clark et al., 1996), or keloids (Akaishi et al., 2010). Clinically and histologically, keloids and hypertrophic scars are distinct tissues (Al-Attar et al., 2006). By describing the composition and structure of tissues and performing mechanical tests, Dunn et al. (1985) have described similar maximum stiffness for hypertrophic scar and normal skin. By touching, hypertrophic scars are commonly appraised as stiffer than normal skin but, in fact, it is not the case and this misperception results from a decreased extensibility. However, high stiffness values on hypertrophic scars have been

noticed by suction tests (Draaijers et al., 2004; Fong et al., 1997) and by extension tests (Clark et al., 1996).

The geometrical shape of keloids depends on the anatomical site (Ogawa, 2008) and this was interpreted as resulting from stress fields and fibers into the skin (Wong et al., 2011). These shapes, except for earlobe keloids (Rockwell et al., 1989), can be read as the consequences of high stresses within the tissue surrounding the scar combined with additional forces (Akaishi et al., 2008a; Ogawa et al., 2012).

The mechano-biological hypothesis for keloid formation has also been tackled from the angle of computational mechanics. By using finite element method, Akaishi et al. (2008b) have simulated an elliptical shaped defect within a plate under tension and obtained the highest stresses associated with the edges of the keloid. This observation is consistent with clinical appearance of butterfly-shaped keloids. Several numerical analyses (Akaishi et al., 2008a; Nagasao et al., 2013) on bi-material *keloid - healthy skin* models have exhibited a correlation between the skin stiffness and the tension generated into the keloid scars. These authors have deduced, first, that low tension in the center of the keloid is related to prevalently better healing and second, a correlation between skin stiffness and the tension level generated in the keloid area. Chambert et al. (2012) have predicted numerically the shape evolution of a presternal keloid. Preliminary results show that the growth of the keloid towards a butterfly shape corresponds to the directions of maximum shear stress.

To the authors' knowledge, no specific apparatus devoted to the mechanical analysis of *in vivo* keloids does exist.

One possibility consists in studying keloids by means of measurement

devices dedicated to *in vivo* skin (de Rigal, 2002; Boyer et al., 2013; Dobrev, 2014; Jacquet et al., 2017b). These devices address in different ways the complexity tied to the skin properties — anisotropic viscous, hyperelastic and prestressed tissue (Xu et al., 2008) — and to the variability of the skin as a function of the body site, the age and the posture of individuals (Flynn et al., 2011; Jacquet et al., 2017a).

Krusche and Worret (1995) have carried out suction tests on keloids at a macroscopic scale in order to evaluate an antikeloidal treatment. Dobrev (1999) performed a mechanical analysis on a single subject with several keloids during cryosurgery by using Cutometer® on keloid and control skin. Wong et al. (2013) have tested a topical stress-shielding device on large hypertrophic scars and modelised their device effect through analyses of strain fields by digital image correlation (DIC) and finite element methods (FEM).

The emergence of the hypothesis that mechano-biological interplay contributes significantly to keloid development suggests that interdisciplinary investigation is necessary to gather diverse biological, structural and mechanical parameters and measurements.

In this aim, this article reports on the *in vivo* investigation of a keloid scar in a young woman. Our analysis is based on diverse non invasive instruments dedicated to *in vivo* skin measurement that cover complementary approaches:

- Optical imaging: photography, optical coherence tomography (Schmitz et al., 2013; Sattler et al., 2013) and confocal microscopy (Gonzalez and Gilaberte-Calzada, 2008; Hofmann-Wellenhof et al., 2012) allow non-invasive sub-surface skin imaging and revealing tissular and even

cellular details, without the need for a skin biopsy ;

- Ultrasound echography providing the skin structure on a depth of a few milimeters (Jemec, 2013) ;

- Mechanical testing by using a commercial device (Cutometer®) and a homemade uniaxial extensometer (Jacquet et al., 2017b).

2. Material and methods

All measurements have been made in temperature and hygrometry regulated rooms (20–22°C, 40-60% relative humidity) after a rest time of 20 minutes.

2.1. Ethical aspects

All the devices used in this study are non-invasive and painless techniques for the patient and do not expose the patient to any particular risk. The subject gave informed written consent to the work. Patient's diagnosis of keloid was confirmed by a surgeon. The patient received no treatment before the measurements. This study abides by the Helsinki Declaration on ethical principles for medical research involving human subjects.

2.2. Description of the clinical case

The keloid specimen (Fig. 1) investigated in the present study was located on the left upper arm (dorsal aspect) of a 22-year-old Caucasian female. The butterfly-shaped keloid scar studied in this paper was 14 mm-width and 47 mm-length. The keloid was composed of a central zone of rectangular shape (21 mm × 7 mm) and two spheroidal nodules (approximate radii of 12 mm and 14 mm) at the extremities. The corresponding area on the right upper arm was considered as contralateral healthy skin

reference zone. Three different sites have been investigated in this study: first the central zone and the largest nodule of the keloid on the left upper arm (subsequently called *keloid*), second the healthy skin zone at approximately 10 mm from the largest nodule of the keloid on the left upper arm (named *surrounding healthy skin* or *SHS*), and third the contralateral side of the keloid on the right upper arm (denoted *contralateral healthy skin* or *CHS*). Additionally, one symmetrical healthy skin zone on both forearms has also been explored as comparative validation tests.

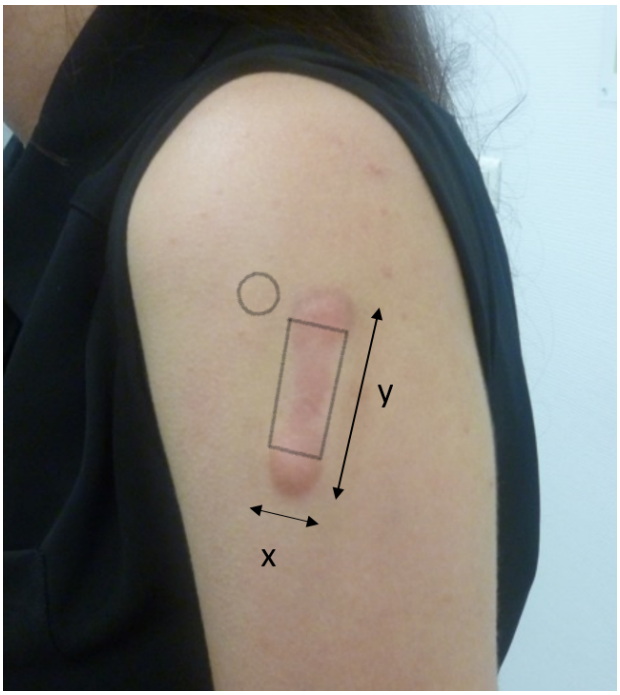

Figure 1: Butterfly-shaped keloid scar on the left upper arm of a 22-year-old woman with $x = 14$ mm and $y = 47$ mm. The central zone of the keloid (surrounding healthy skin, respectively) is delimited by a rectangular (circle, respectively).

2.3. Imaging techniques

2.3.1. Photography and video recording

The purpose of standardized photography is to control image input by avoiding position or slight shifts of the camera, the subject or environment. Standardized photos in normal light have been performed using a Canon PowerShot® SX510 HS camera, including overview and close-up photos. The UI-2230SE-C camera (IDS Imaging Development Systems GmbH) has been used to measure the fields of displacement by means of digital image correlation (DIC).

2.3.2. Ultrasound echography

Specific high frequency ultrasound probes have been applied on the keloid scar surface (with water gel to adapt impedance between skin/probe): 20 MHz (Atys Dermcup®, DUB® SkinScanner TPM) and 50 MHz (DUB® SkinScanner TPM). Different structures appear in skin echography and characterize the dermis layer:

- Structures with low echogenicity are water-filled tissues (inflammation) or with low fibrillar density (superficial dermis).
- Structures with high echogenicity are rich in collagen.

By longitudinal scanning of the skin surface, successive signal lines have been obtained and used to reconstruct cross section images of the skin. Then skin states have been assessed through dermis density and homogeneity of structures. Skin thickness, considered as the thickness of epidermis and dermis layers, has been measured perpendicularly to the skin surface at three sites: keloid, surrounding healthy skin and contralateral healthy skin. An average value of three measurements has been carried out at each site.

2.3.3. Optical Coherence Tomography (OCT)

Keloid and healthy skin have been observed by OCT that allows an investigation of the different skin layers in real time without being invasive for the patient though a real "optical biopsy". The Vivosight® instrument (Michelson Diagnostics) is based on the reflection of light waves and allows an exploration of the architecture of the skin in epidermal and dermal layers (up to a depth of about 1.5 mm). A light beam (wavelength of 1300 nm) is directed to the skin areas of interest, where it scattered in depth. Depending on tissue characteristics, images will appear more or less contrasted. Tomography is used to reconstruct in real-time the 2D elements observed in the sagittal and transverse planes, and permit even to obtain 3D reconstructions. OCT provides relevant information on contrast between epidermis and dermis, epidermis homogeneity and thickness, homogeneity of papillary dermis layer, associated vasculature, homogeneity of reticular dermis, and possible mottling structure (collagen).

2.3.4. Confocal microscopy

Three dimensional structure of skin can be reconstructed by confocal microscopy from sets of images recorded at different depths. Keloid and healthy skins have been evaluated by confocal microscopy (Vivascope® 1500 MAVIG) that is a non invasive method used to observe through the epidermis (and superficial dermis). A specific ring with glasses, oil and gel (impedance) is applied on the skin, and allows attachment with laser head: near infrared beam (wavelength of 830 nm) is directed through a series of lenses and a beam splitter, toward skin and reflected by the investigated areas. Melanin and keratin are like natural contrast agents because of their relatively high reflection index. The microstructures of the skin can be rep-

resented in square images parallel to the skin surface at different depths. Black and white images (500 μm $\times$ 500 μm) of each cutaneous layer are produced and visualized instantly. The skin structure can thus be investigated layer by layer up to a maximum depth of 200-250 μm. For this keloid evaluation, quality of the surface layers will be explored, through epidermis structures thickness, signs of inflammation (spongiosis, vesicles, infiltration), pigmentation, dermal-epidermal junction (papillae and capillaries) and collagen structure.

2.4. Mechanical investigations

2.4.1. Cutometry

The SEM 575 Cutometer® (Courage & Khazaka Electronic GmbH, Cologne, Germany) has been used to measure the biomechanical properties of the skin *in vivo* by a suction test (Dobrev, 2014; Berndt and Elsner, 2002; O'Goshi, 2006). A measuring probe of 6 mm-diameter has been placed on the skin and a negative pressure of 400 mbar has been applied during 3 seconds, then a relaxation time has been performed during 2 seconds, and this cycle has been repeated 3 times to test the fatigability of the skin. Adhesive tape has been attached to the probe and prevents the adjacent skin from being sucked into the chamber. An optical system made of a light source and a receptor determines the penetration depth of skin.

The parameters extracted from the evolution curve of skin deflection versus time (Fig. 2) are U_e (immediate distension), U_v (delayed distension), U_f (final distension), U_r (immediate retraction) and U_a (final retraction). Then, the R-parameters are computed as follows: $R_0 = U_f$ (skin distensibility), $R_1 = U_f - U_a$ (resilient distension), $R_2 = U_a/U_f$ (gross elasticity including viscous effects), R_3 (last maximum amplitude), R_4 (last minimum

amplitude), $R_5 = U_r/U_e$ (net elasticity without viscous effects), $R_6 = U_v/U_e$ (viscoelasticity ratio), $R_7 = U_r/U_f$ (biological elasticity) $R_8 = U_a$ and $R_9 = R_3 - R_0$. Skin elasticity is related to parameters U_e, U_r, R_0, R_2, R_5 and R_7; skin viscoelasticity is linked to parameters U_v and R_6; and skin fatigability is represented by R_9-parameter (Dobrev, 2014).

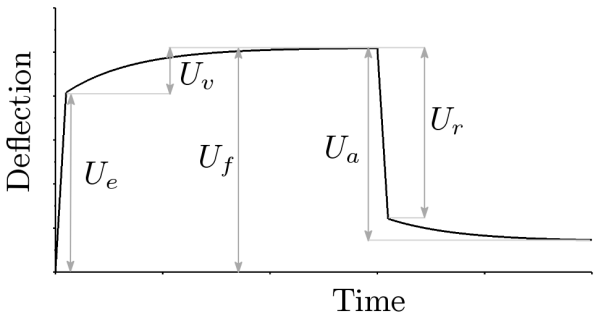

Figure 2: Evolution curve of skin deflection versus time with parameters obtained from the suction test with the Cutometer®.

2.4.2. Extensometry

Uniaxial extension measurements are obtained by using an ultra-light homemade portable extensometer (Fig. 3) which is a research prototype that minimizes the skin disturbances induced by the skin surrounding the tested zone (Jacquet et al., 2017b). Skin extension is performed by a set of two double-pads: one is fixed to the portable frame while the other is moved along guiding columns by means of an electric motor. The double-pads are composed of a central pad surrounded by a 'U-shaped' guarding one. Measurements are retrieved from the central pad only. The guarding pads apply the same extension to the surrounding skin with the aim of minimizing disturbances from non-loaded skin. Extension tests are servo-controled either in force or displacement. Tests are synchronized with the

recording of measurements provided by dedicated sensors. The displacement sensor (LVDT-type sensor) provides the mobile pad position. The force sensor is a bronze-beryllium cantilever equipped with strain gauges stuck on the sensor. The initial distance between the fixed and mobile pad is about 31 mm. The two double-pads are fixed onto the skin by means of a surgical adhesive used in dermatological surgery.

The proposed methodology consists in testing the keloid located on the left upper arm and the healthy skin situated on the symmetrical-zone of the right upper arm. This methodology will be discussed at the beginning of Subsection 3.2.2 by comparing the force-displacement responses of one healthy-skin zone investigated symmetrically on both forearms.

The applied test consists of three loading-unloading repetitions at a controlled speed of 1 mm/s (Fig. 4). The maximum displacement applied for healthy skin and keloid has been determined from literature (Dobrev, 1999; Dunn et al., 1985). The mechanical displacement field is tracked continuously by means of digital image correlation (Eberl et al., 2010). Images are obtained thanks to a camera which stands independently of the extensometer above the solicited area of skin. A speckle pattern is applied onto the skin to improve image correlation. Slight motions of the subject are automatically compensated by following the position of the extensometer frame within recorded images.

The extension test provides the force exerted on the measurement pads and the imposed displacement between the two pads as a function of time. The skin preconditioning is highlighted by a decrease of the force response across the three successive loadings. The mechanical analysis has been performed using the results obtained from the three consecutive loadings.

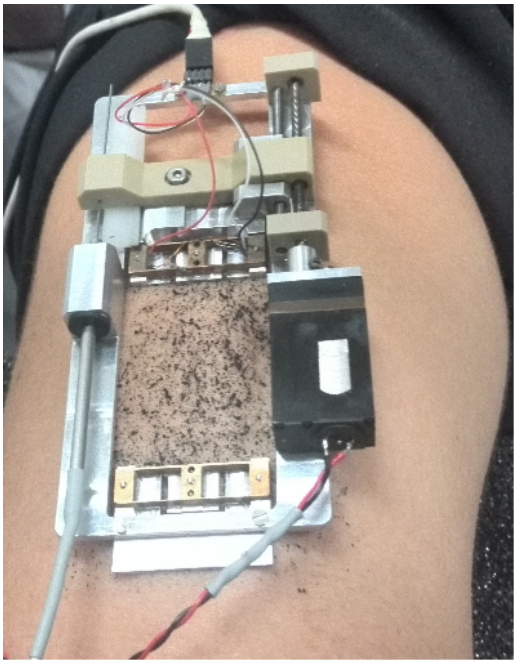

Figure 3: Photo of the extensometer on the keloid with a speckle pattern. The details of the device have been described in Jacquet et al. (2017b).

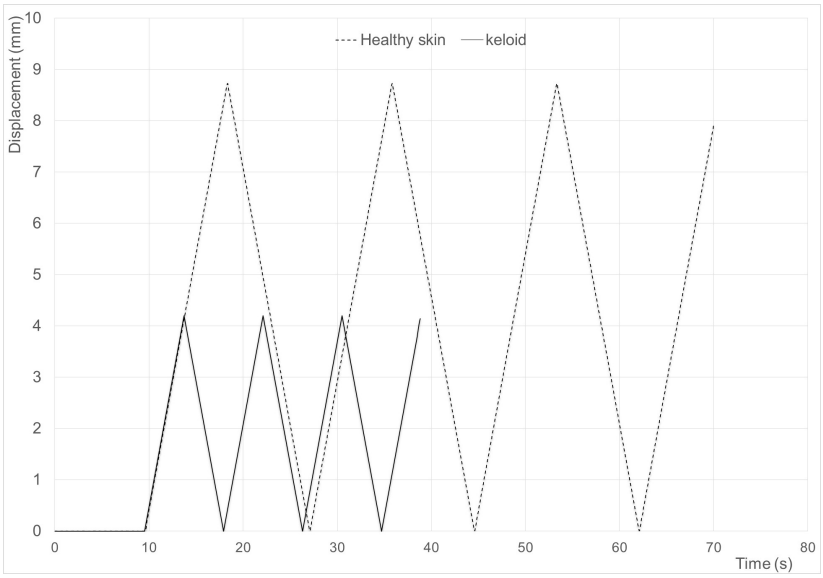

Figure 4: Input commands with controlled displacement speed for CHS and keloid scar.

The proposed extension test can be considered as similar to a classical traction test (Jacquet et al., 2017b). The mechanical behavior of skin tissue is characterized by experimental stress–strain curve, which results from the measurements of force and displacement recorded during the extension test. The uniaxial engineering stress along the traction direction is defined by:

$$T = \frac{F}{A_0} = \frac{F}{d \cdot e_0} \ , \tag{1}$$

where F is the measured force, A_0 is the initial cross-sectional area of the specimen, d is the width of measuring pad and e_0 is the initial skin thickness. The uniaxial engineering strain in the loading direction is given by:

$$\varepsilon = \frac{\Delta L}{L_0} = \frac{L - L_0}{L_0} \ , \tag{2}$$

where ΔL is the displacement of the movable measuring pad; L and L_0 are respectively the current and initial lengths between the two pads.

As in Jacquet et al. (2017a), three physical parameters are identified from the stress-strain curve using a non-linear least squares method:

- the initial tangent modulus E_1 (initial slope of the stress–strain curve) which corresponds to the contribution of the elastin fibers alone (Raghavan et al., 1996),

- the final tangent modulus E_2 (final slope of the stress–strain curve) which stands for the combined contribution of elastin and collagen fibers (Raghavan et al., 1996),

- the intercept ε_T of the strain-axis with the final slope of the stress–strain curve which can be interpreted as a characteristics of skin extensibility (Gibson et al., 1969).

3. Results and analysis

3.1. Structural imaging analysis

3.1.1. Ultrasound echography

Skin imaging through ultrasound provides information about general organization of the tissues. Images obtained on the healthy area present a well-defined interface between dermis and epidermis, regular and hyper echogenic dermis layer (indicated on Fig. 5-left with a red asterisk); border with dark hypodermis is clear-cut (indicated on Fig. 5-left with a red arrow), and density of the dermis is homogenous (Fig. 5-left).

By contrast, dermis and the transition with hypodermis in keloid images (Fig. 5-right) are no longer identified, as pathological tissue seems to invade the whole area. The convex shape of this image results from the application of the probe transversally to the scar. The pathological scar presents an ovoid shape with heterogeneous echogenicity throughout the whole width of the scar.

Average value of skin thickness has been measured by echography at three sites: 1.46 $\pm$ 0.1 mm for the contralateral healthy skin, 1.34 $\pm$ 0.05 mm for the surrounding healthy skin and 2.93 $\pm$ 1.26 mm for the keloid. A large standard deviation of skin thickness is obtained for the keloid because the skin thickness is not constant along the keloid, and the measurements have been taken at the dome of keloid nodule and besides the nodule.

3.1.2. OCT

On the control skin area (Fig. 6-left), OCT offers a classical view of a healthy architecture, with a first epidermis layer showing regular surface and density (epidermis marked with a red asterisk), clearly separated from dermis (indicated with red arrows). Below, dermis presents some dark

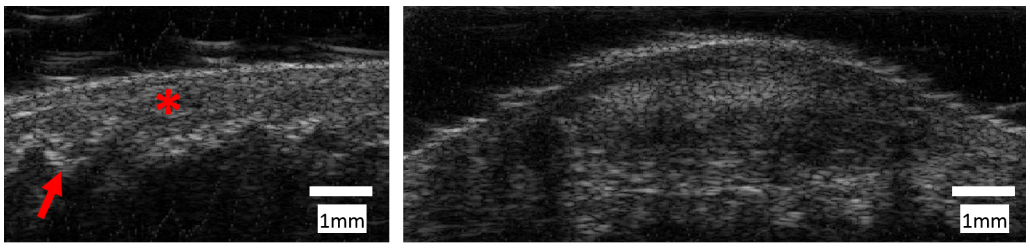

Figure 5: Ultrasound observation of healthy skin (left) with regular dermis+epidermis and hyper echogenic layer marked with a red asterisk, as well as clear identified border with dark hypodermis indicated with a red arrow; and keloid scar (right) characterized by ovoid shape without distinction of the different layers.

structures and hyper bright ones, suggesting respectively a normal vascular network and an organized collagen pattern.

On the keloid area (Fig. 6-right), OCT exploration confirms the loss of regular surface as well as distinction and contrast between the first two layers of the skin. Fine vessels are distributed on the whole skin coat, irregularly. The general darker aspect of the image could express a liquid infiltration, kind of oedema due to inflammation.

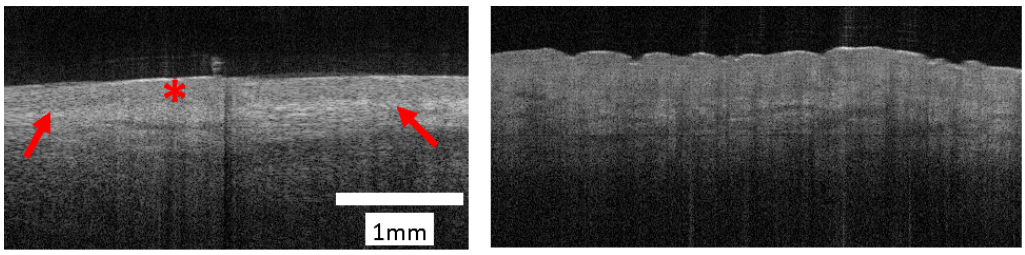

Figure 6: OCT observation of healthy skin (left): epidermis layer marked with a red asterisk, clearly separated from dermis indicated with red arrows; and keloid scar (right): irregular surface, difficult distinction of epidermis/dermis border, dark area suggesting liquid infiltration.

3.1.3. Confocal microscopy

Reflectance confocal microscopy offers subsurface images of the skin in a transversal view (horizontal section, Fig. 7), at a cellular level but up to

a limited depth (up to 200 μm). These observations define the quality of the skin epidermis as healthy when, from surface to deepness:

- bright *stratum corneum* is the first layer that appears when confocal examination starts; it is constituted with cells (polygonal corneocytes 10-30 μm) clustered and surrounded by visible skin dark folds, or skin marks, furrows, or dematoglyphs (Fig. 7 top left, red arrows);

- *stratum granulosum* and *spinosum* described as honeycomb pattern of polygonal granular then spinous keratinocytes;

- dermal epidermal junction shows dark dermal papillae rings, surrounded or topped by bright melanocytes or pigmented keratinocytes (7-12 μm), and centered by capillary loops allowing to observe blood cells flow; this structure is characteristic from the undulating junction, with "finger-like" projections of dermis into the epidermis (Fig. 7 down left and right, red arrows).

What is remarkable is that we can observe obvious differences when exploring the pathological area. At the comparable depths of exploration, pathological scar epidermis looks as modified in its layer aspect, as if the tissue was inflated. In this way surface furrows (dark lines clearly observed in control area) disappeared or are clearly diminished in term of width (Fig. 7 top right, red arrows); on the same way and still resulting from this "inflated" appearance, thicknesses of the strata seems increased : at the sam depths of observation it is clear that observed cells clusters and characteristics on the pathological images correspond in what is usually observed in deeper regions in healthy skin. Indeed, in the example of (Fig. 7) at 20 μm we only

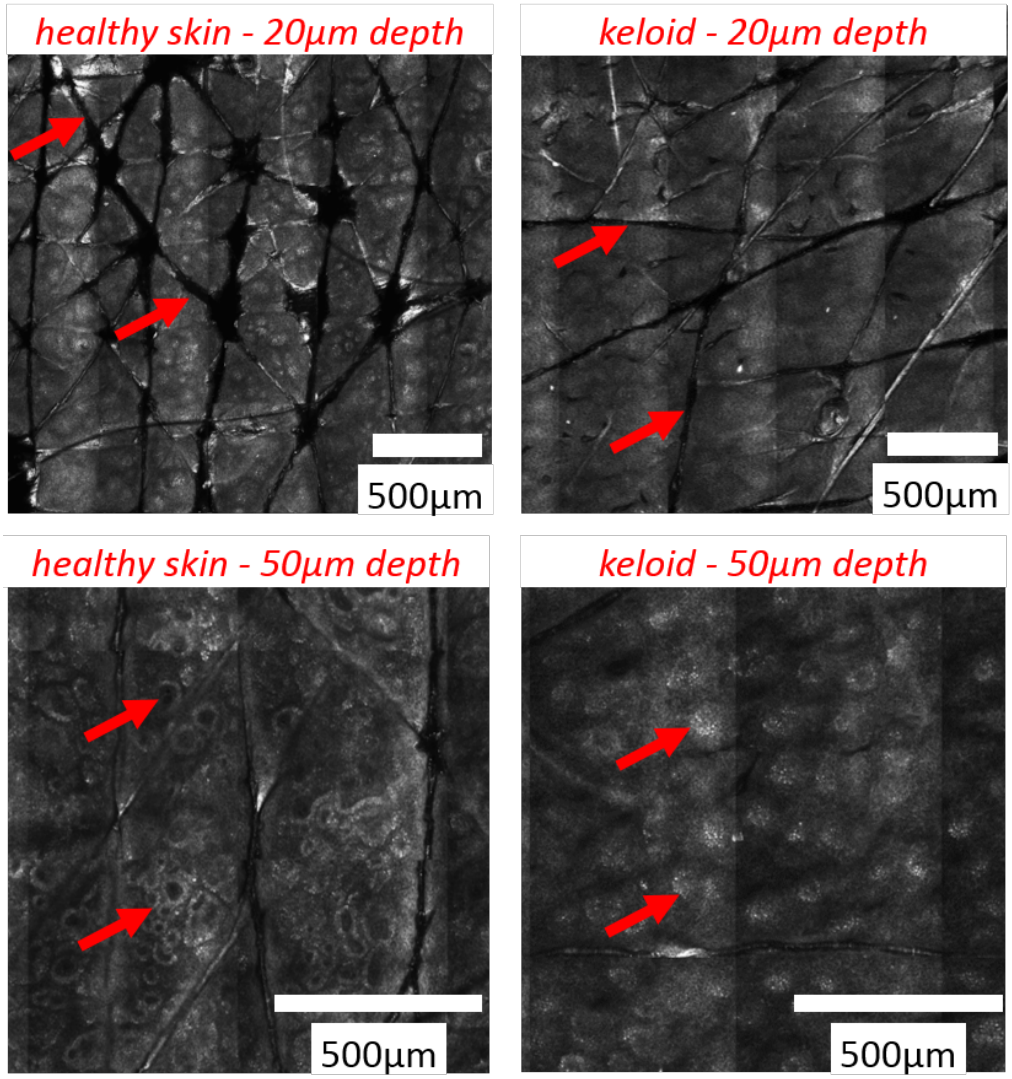

Figure 7: Reflectance confocal images of skin in transversal view at a depth of 20 μm (top) and 50 μm (bottom): -healthy skin: left top *stratum corneum* with large dark furrows (red arrows) and "honeycomb" pattern, left down with papillae rings surrounded by bright melanocytes (red arrows), -and keloid scar: right top with thinner folds (red arrows).

observe what could be the deeper "end" of the furrows, while at 50 μm we can see the top of the undulating dermal epidermal junction.

On the observation of the lesion areas, signs also described in the literature as patterns of inflammation are visible : disarrayed *stratum spinosum* aspect of honeycomb, *spongiosis* (large dark intercellular spaces), interface changes, dilated vessels on the deeper view.

3.2. Mechanical results

3.2.1. Cutometry

As shown in Fig. 8, clinical examination by cutometry exhibits different mechanical behaviors for keloid, surrounding healthy skin (SHS) and contralateral healthy skin (CHS). The parameters retrieved by cutometry are listed in Table 1. The elastic parameters, viscoelastic parameters and fatigability parameter are analyzed separately.

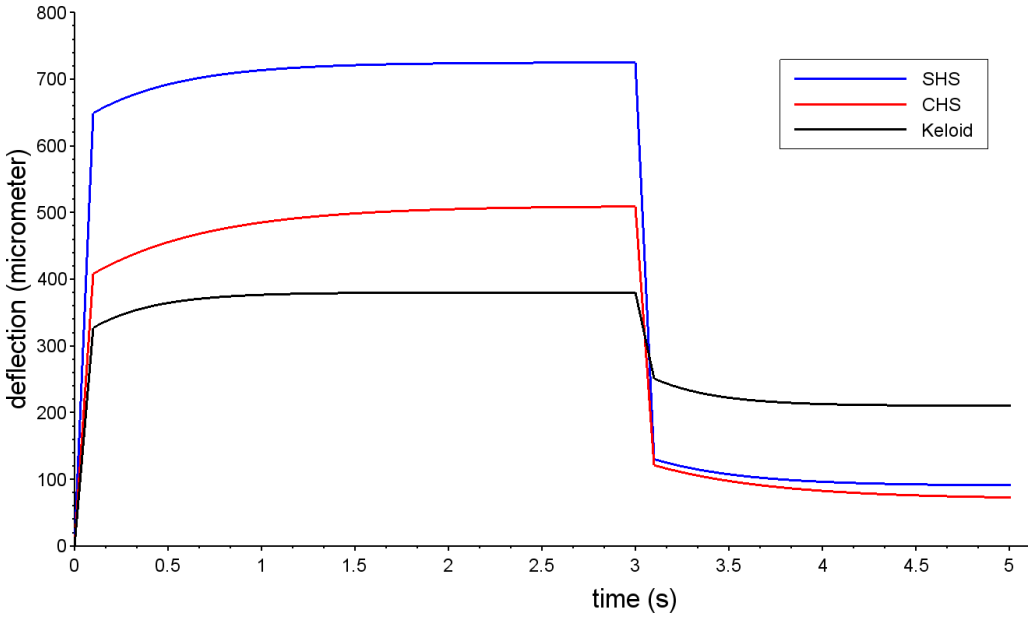

Figure 8: Evolution curve of deflection versus time for keloid, surrounding heathly skin (SHS) and contralateral healthy skin (CHS) with 6-mm diameter probe.

As far as elasticity is concerned, each parameter value is higher in healthy skin (SHS and CHS) than in keloid. More precisely, the parameters U_e, R_0, R_2, R_5 and R_7 are approximately twice higher in surrounding healthy skin (SHS) than in keloid except for the U_r-parameter that is more than four times higher. Each elastic parameter value in the contralateral healthy skin (CHS) is higher than the keloid one but in a lesser degree than in SHS. The three parameters R_2, R_5 and R_7 have quite similar values in CHS and SHS and more than twice higher than the keloid ones.

Parameter	Unit	Keloid	SHS	CHS
U_e	μm	330	650	410
U_v	μm	50	75	100
U_r	μm	130	595	390
$U_a = R_8$	μm	170	635	440
$U_f = R_0$	μm	380	725	510
$U_a - U_r$	μm	40.0	40.0	50.0
$(U_a - U_r)/U_v$	—	0.8	0.533	0.5
$R_1 = U_f - U_a$	μm	210	90.0	70.0
$R_2 = U_a/U_f$	—	0.447	0.877	0.863
R_3	μm	400	670	480
R_4	μm	260	80	80
$R_5 = U_r/U_e$	—	0.394	0.915	0.951
$R_6 = U_v/U_e$	—	0.15	0.12	0.244
$R_7 = U_r/U_f$	—	0.342	0.821	0.765
$R_9 = R_3 - R_0$	μm	20.0	55.0	30.0

Table 1: Parameters values obtained by cutometry on the keloid, surrounding healthy skin (SHS) and contralateral healthy skin (CHS).

Concerning the viscoelasticity, the parameter U_v has higher values in CHS and SHS than in the keloid, although the keloid R_6-value is between SHS and CHS values. Let consider the delayed retraction as the difference between U_a and U_r and the net viscosity ratio between the delayed retraction

to the delayed distension (U_v). The values of $U_a - U_r$ are in the same order of magnitude for keloid, SHS and CHS. The net viscosity ratio values are quite the same in CHS and SHS (0.5) and higher (0.8) in keloid.

The value of fatigability represented by R_9-parameter is 1.5 times higher in CHS than in keloid and three times higher in SHS than in keloid.

3.2.2. Extensometry

As validation test, one healthy-skin zone has been investigated symmetrically on both forearms (anterior aspect) of the clinical case. Fig. 9 shows the force-displacement curves of three successive loadings on one zone located symmetrically on both forearms. For each loading, the curves for right and left forearms are not identical. However, they present a common shape and differ only in magnitude. The difference of magnitude bears witness of the intra-individual variability of the skin mechanical properties. Nevertheless, because of the common shape observed and keeping in mind the observed discrepancy of magnitude, the contralateral zone can be considered as an acceptable qualitative healthy-skin reference to appraise the mechanical behavior of keloid.

The force during three consecutive loadings versus displacement have been obtained for contralateral healthy skin (CHS) and keloid. It should be noted that the surrounding healthy skin (SHS) has not been tested by extensometry because the sizes of SHS and measuring area are unbalanced. Fig. 10 represents the stress-strain curves corresponding to three consecutive loadings for CHS and keloid (see Fig. 4).

The stress-strain curves show higher stiffnesses of keloid than CHS ones. The CHS extensibility is about twice larger than the keloid one.

The maximum of the loading on healthy skin is not sufficient to submit

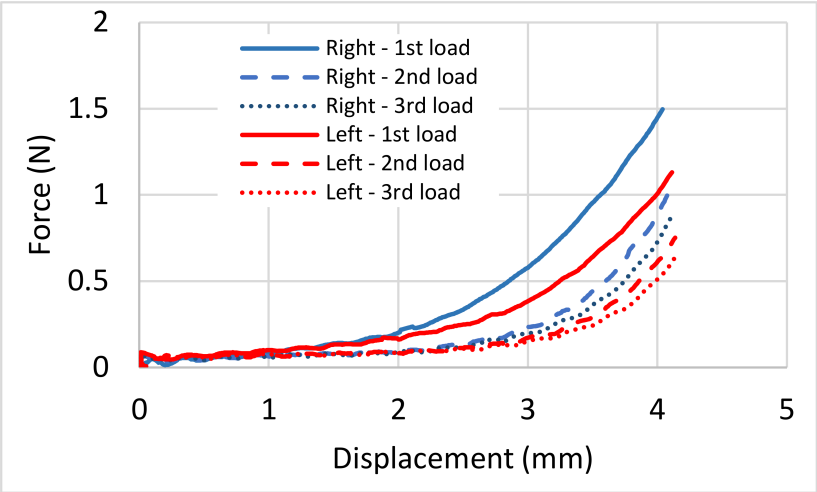

Figure 9: Force-displacement curves for right and left symmetrical sites on forearms for three successive loadings.

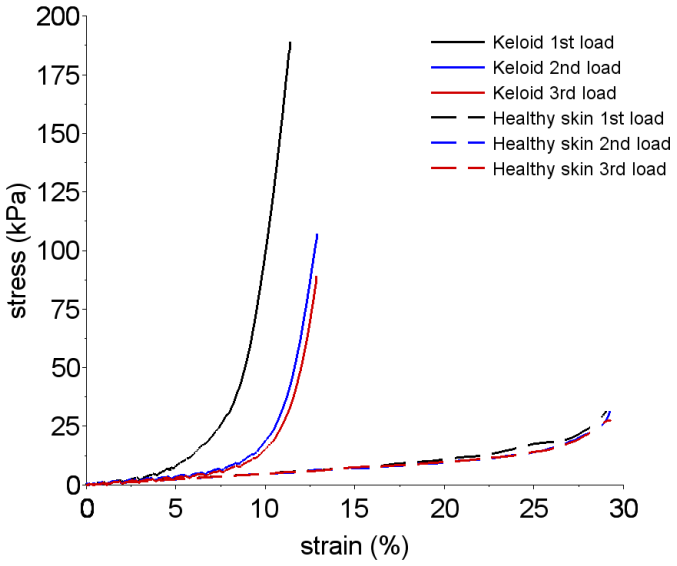

Figure 10: Stress-strain curves for keloid and contralateral healthy skin (CHS) for three consecutive loadings.

the skin to high strain level and the force response of healthy skin remains in the low values. The same displacement rate conditions are imposed to the two materials and the test on the keloid lasted less longer than the one on healthy skin that reached higher strains.

For keloid, the curve at the first loading is different from the second and the third ones which are quite similar: this illustrates the pre-conditionning of the skin. For CHS, the curves for the three loadings are close together because the toe region of the skin has not been exceeded.

The values of the physical parameters E_1, E_2 et ε_T for keloid and CHS are listed in Table 2. In the following, we remain aware that the comparison between keloid and CHS is qualitatively relevant, but quantitatively approximate because of intra-individual variability in the mechanical behavior of the skin. As far as initial tangent modulus E_1 is concerned, the keloid values are higher than the CHS ones. At the third loading, the keloid E_1-parameter value is equal to 60 kPa and the CHS one is equal to 47 kPa, i.e. an increase of about 27 %. Concerning the final tangent modulus E_2, the keloid value is very high compared to the E_1 value. At the third loading, keloid E_2 is equal to 5 MPa which is approximately one hundred times higher than the E_1 value. Concerning the threshold ϵ_T, the keloid value is around 11 % at the third loading and the CHS value (26 %) is more than twice higher. The E_2 and ϵ_T values for CHS have been determined even if the final phases of stress-strain curves have not been reached. So the corresponding final tangent modulus and threshold values for CHS are underestimated.

The displacement fields of the zone of interest have been identified by digital image correlation (Fig. 11). X-displacement field along the direction

Site	Load	E_1 (kPa)	E_2 (kPa)	ε_T (%)
Keloid	1st	121	6 756	8.8
	2nd	61	4 884	11.0
	3rd	60	5 032	11.3
CHS	1st	48	400*	27.5*
	2nd	47	608*	28.2*
	3rd	47	258*	26.1*

Table 2: Physical parameters values obtained by extensometry on the keloid and contralateral healthy skin (CHS) for three consecutive loadings. The symbol * is used for underestimated values.

of the extension (X-axis) is illustrated in Fig. 11a for keloid and Fig. 11b for CHS. The X-displacement field for CHS is linearly distributed along the X-axis contrary to the one observed for keloid. For a given X-position, the X-displacement between the two central pads for CHS is quite uniform except for a few scattered marks due to experimental artefacts.

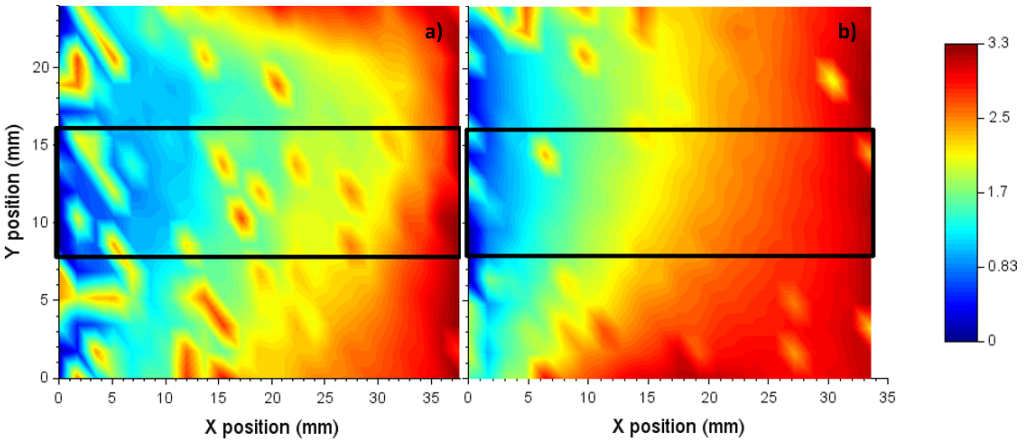

Figure 11: X-displacement fields (values in mm) at about 10 % strain within keloid (a) and contralateral healthy skin (b).

4. Discussion

The presented results report on a structural and mechanical investigation of a single case of *in vivo* keloid using medical imaging, cutometry and extensometry techniques. The systematic comparison of the results obtained on the keloid with those obtained on the healthy skin of the same individual reinforces the relevance to this study even if this comparison is qualitative due to the zone dependency of the mechanical properties of the human skin.

From ultrasound and OCT imaging results, and as described by Limandjaja et al. (2017), epidermis seems more flattened in keloid than in healthy skin : the anatomical limit between dermis and epidermis disappears in keloid.

From a mechanical standpoint, our article reports on the first experimental results obtained on keloid by extensometry *in vivo*. The main particularities of the *in vivo* device used is to overcome the influence of the neighboring skin on the measured zone (Jacquet et al., 2017b) thanks to additional guarding pads and its ultra-light weight.

In order to compare the healthy skin with keloid, the contralateral side of keloid has been chosen as the most relevant healthy-skin reference keeping in mind that a magnitude difference has been observed between the healthy skins of both forearms. Assessing the mechanical behaviors of keloid and healthy-skins (CHS and SHS) by using cutometry and extensometry, the keloid stiffness is clearly higher than the healthy skin ones, both at the beginning of the loading (E_1) and at the end of the loading (E_2). This has been noticed similarly within hypertrophic scars from suction tests (Draaijers et al., 2004; Fong et al., 1997) and extension tests (Clark et al., 1996).

In our study, after pre-conditionning, the initial tangent elastic modulus (initial stiffness) at the third loading, is about 1.28 times higher in keloid (60 kPa) than in contralateral healthy skin (CHS : 47 kPa). This ratio is close to the one obtained by Dunn et al. (1985) on hypertrophic and control healthy skin based on the maximum stiffness values (2011/1586 $\approx$ 1.27). The same analysis concerning the threshold strain ϵ_T (Keloid: 11.3 % and CHS: 26.1 %) produces a ratio equal to 0.43, although the ratio of strain at maximum stiffness is equal to 0.46 ($\approx$ 0.4 % for hypertrophic scar divided by 0.87 % for control skin) in Dunn et al. (1985).

As shown in Table 3, our results are not too far from Dobrev's ones for the final distension R_0, the viscoelastic ratio R_6 and the biological elasticity R_7. Nevertheless, the comparison of relative gaps between these two studies is not fully relevant. Indeed, the discrepancies between the relative gaps can be related to the clinical grading of scar tissue (Clark et al., 1996) and the parameters of the Cutometer® (probe diameter, time durations of suction and relaxation).

Retative gap	Dobrev (1999)	Present results
$(R_0^{\mathrm{K}} - R_0^{\mathrm{HS}})/R_0^{\mathrm{HS}}$	-59 %	-48 %
$(R_6^{\mathrm{K}} - R_6^{\mathrm{HS}})/R_6^{\mathrm{HS}}$	$+163$ %	$+131$ %
$(R_7^{\mathrm{K}} - R_7^{\mathrm{HS}})/R_7^{\mathrm{HS}}$	-23 %	-58 %

Table 3: Relative gaps of results extracted from Dobrev (1999) and present results. Dobrev uses a SEM 474 Cutometer® with a 8 mm-diameter probe under 400 mbar during 5 s followed by a 5 s relaxation time. The present results come from a SEM 575 Cutometer® with a 6 mm-diameter probe under 400 mbar during 3 s followed by a 2 s relaxation time. Superscripts "K" and "HS" mean, respectively, keloid and healthy skin.

According to Dobrev (2014), the use of a 8 mm-diameter probe is appropriate to evaluate the mechanical properties of the whole skin (dermis and

hypodermis) of skin diseases such as keloids. A 6 mm-diameter aperture, which is used in our study, enables to determine the mechanical properties of the skin outer layers.

Otherwise, after the toe-region phase of keloid behavior, a small strain increment entails a large stress increment due to a significant increase in stiffness. In the stress-strain curve, the uniaxial mechanical stress within the keloid has been determined by assuming an homogeneous mean value of the initial thickness of keloid which have been measured by echography. But in fact, the keloid topography is highly rugged and the thickness should not be considered as constant. The keloid thickness is greater than the healthy skin one. Despite of higher values of the keloid tangent moduli, our results do not show higher final stiffness within keloid with respect to the healthy skin one. Like in Dunn et al. (1985) for hypertrophic scar tissues *ex vivo*, our results highlight a lower extensibility of the keloid scar than the healthy skin. Contrary to Dunn et al. (1985), it can not be concluded that the maximum stiffness of keloid and skin are similar.

The size of the loaded area is very different for both tests: cutometry ($\pi \times 3^2 \approx 28$ mm^2) and extensometry ($24 \times 31 \approx 744$ mm^2). Both tests act on the skin surface in different ways: normally to the surface for cutometry assimilated with biaxial traction and tangentially to the surface for extensometry similar to uniaxial traction. Within the depth of the skin, both tests reveal shear stress components due to subcutaneous fascias. Considering the mobility of the skin, shearing is neglected in extensometry. Regarding the suction test, the skin is submitted to biaxial traction and shearing. As a consequence, a stiffness of skin or keloid based on the measurements obtained by cutometry, is influenced by these subcutaneous tissues, and

thus this stiffness is not comparable to the one resulting from extensometry. Nevertheless, the extensibility values from suction and extension tests are higher for healthy skin (SHS and CHS) than for keloid.

5. Conclusion

This multimodal investigation constitutes an exploratory study of a keloid scar by combining diverse non invasive techniques dedicated to *in vivo* skin measurement: optical imaging (OCT and confocal microscopy), ultrasound high resolution echography, cutometry and extensometry. These preliminary results will form the bases for a larger clinical investigation.

Contrary to healthy skin, keloid is not composed of well-defined layers. A flattening of dermal-epidermal junction and a skin thickening have been observed on keloid in comparison with healthy skin.

The extensibility of keloid is highly lower than that of healthy skin. Also, the initial rigidity of keloid is higher than the one of healthy skin. To compare the final rigidity of keloid versus healthy skin, further tests have to be proceeded with higher strain value.

Knowing the intrinsic mechanical parameters of both healthy skin and keloid, the numerical analysis of the bi-material structure by using the finite element method paves the way for identifying the most likely directions of keloid growth.

To date, there is no standard method to objectively assess therapeutic outcomes after keloid treatment. As shown here, a multimodal approach could lead to quantitatively better characterize keloid scars not only after diagnosis but also after treatment. The combination between imaging and biomechanics could provide a new kind of decision support tool for surgeons.

Moreover, being able to collect such data over time is challenging and could potentially help to anticipate keloid formation or evolution.

Acknowledgments

This work was supported by European Union FEDER grant from Région Bourgogne Franche-Comté, France (no. 36381). The authors acknowledge insightful reviewers' comments that resulted in significant paper improvement.

Conflict of Interest

The authors declare that they have no conflict of interest.

References

Akaishi, S., Akimoto, M., Ogawa, R., Hyakusoku, H., 2008a. The relationship between keloid growth pattern and stretching tension: visual analysis using the finite element method. Ann. Plast. Surg. 60, 445–451.

Akaishi, S., Ogawa, R., Hyakusoku, H., 2008b. Keloid and hypertrophic scar: neurogenic inflammation hypotheses. Med. Hypotheses 71, 32–38.

Akaishi, S., Ogawa, R., Hyakusoku, H., 2010. Visual and pathologic analyses of keloid growth patterns. Ann. Plast. Surg. 64, 80–82.

Al-Attar, A., Mess, S., Thomassen, J. M., Kauffman, C. L., Davison, S. P., 2006. Keloid pathogenesis and treatment. Plast. Reconstr. Surg. 117, 286–300.

Atkinson, J.-A. M., McKenna, K. T., Barnett, A. G., McGrath, D. J., Rudd, M., 2005. A randomized, controlled trial to determine the efficacy of paper tape in preventing hypertrophic scar formation in surgical incisions that traverse Langer's skin tension lines. Plast. Reconstr. Surg. 116, 1648–1656.

Bayat, A., McGrouther, D. A., Ferguson, M. W. J., 2003. Skin scarring. BMJ: Br. Med. J. 326, 88–92.

Berndt, U., Elsner, P., 2002. Hardware and measuring principle: The Cutometer®. In: Elsner, P., Berardesca, E., Wilhelm, K.-P., Maibach, H. I. (Eds.), Bioengineering of the Skin: Skin Biomechanics. Vol. V. CRC Press, Ch. 7, pp. 91–97.

Boyer, G., Molimard, J., Ben Tkaya, M., Zahouani, H., Pericoi, M., Avril, S., 2013. Assessment of the in-plane biomechanical properties of human skin using a finite element model updating approach combined with an optical full-field measurement on a new tensile device. J. Mech. Behav. Biomed. Mater. 27, 273–282.

Butler, P. D., Longaker, M. T., Yang, G. P., 2008. Current progress in keloid research and treatment. J. Am. Coll. Surg. 206, 731–741.

Cerda, E., 2005. Mechanics of scars. J. Biomech. 38, 1598–1603.
Chambert, J., Zhao, L., Remache, D., Jacquet, E., 2012. Numerical analysis of keloid scar in the presternal area. Comput. Method. Biomech. Biomed. Eng. 15 (Suppl. 1), 23–24.
Chike-Obi, C. J., Cole, P. D., Brissett, A. E., 2009. Keloids: pathogenesis, clinical features, and management. Semin. Plast. Surg. 23, 178–184.
Clark, J. A., Cheng, J. C. Y., Leung, K. S., 1996. Mechanical properties of normal skin and hypertrophic scars. Burns 22, 443–446.
Daya, M., 2011. Abnormal scar modulation with the use of micropore tape. Eur. J. Plast. Surg. 34, 45–51.
de Rigal, J., 2002. Hardware and basic principles of the dermal torque meter. In: Elsner, P., Berardesca, E., Wilhelm, K.-P., Maibach, H. I. (Eds.), Bioengineering of the Skin: Skin Biomechanics. Vol. V. CRC Press, Ch. 5, pp. 63–76.
Dobrev, H., 1999. Non-invasive monitoring of the mechanical properties of keloids during cryosurgery. Acta Derm. Venereol. 79, 487–488.
Dobrev, H., 2014. Cutometer®. In: Berardesca, E., Maibach, H. I., Wilhelm, K.-P. (Eds.), Non Invasive Diagnostic Techniques in Clinical Dermatology. Springer, Ch. 29, pp. 315–338.
Draaijers, L. J., Botman, Y. A. M., Tempelman, F. R. H., Kreis, R. W., Middelkoop, E., van Zuijlen, P. P. M., 2004. Skin elasticity meter or subjective evaluation in scars: a reliability assessment. Burns 30, 109–114.
Dunn, M. G., Silver, F. H., Swann, D. A., 1985. Mechanical analysis of hypertrophic scar tissue: structural basis for apparent increased rigidity. J. Investig. Dermatol. 84, 9–13.
Eberl, C., Thompson, R., Gianola, D., Bundschuh, S., 2010. Digital Image Correlation and tracking with Matlab. Tech. rep., Matlab Central File Exchange.
URL www.mathworks.com/matlabcentral/fileexchange/12413-digital-image-correlation-and-tracking
Flynn, C., Taberner, A., Nielsen, P., 2011. Measurement of the force–displacement response of *in vivo* human skin under a rich set of deformations. Med. Eng. Phys. 33, 610–619.
Fong, S. S. L., Hung, L. K., Cheng, J. C. Y., 1997. The cutometer and ultrasonography in the assessment of postburn hypertrophic scara preliminary study. Burns 23 (Suppl. 1), S12–S18.
Fraccalvieri, M., Sarno, A., Gasperini, S., Zingarelli, E., Fava, R., Salomone, M., Bruschi, S., 2013. Can single use negative pressure wound therapy be an alternative method to manage keloid scarring? A preliminary report of a clinical and ultrasound/colour-power-doppler study. Int. Wound J. 10, 340–344.
Gibson, T., Stark, H., Evans, J. H., 1969. Directional variation in extensibility of human skin *in vivo*. J. Biomech. 2, 201–204.
Gonzalez, S., Gilaberte-Calzada, Y., 2008. In vivo reflectance-mode confocal microscopy in clinical dermatology and cosmetology. Int. J. Cosmet. Sci. 30, 1–17.
Hofmann-Wellenhof, R., Pellacani, G., Malvehy, J., Soyer, H. P., 2012. Reflectance confocal microscopy for skin diseases. Springer Science & Business Media.
Huang, C., Akaishi, S., Hyakusoku, H., Ogawa, R., 2014. Are keloid and hypertrophic scar different forms of the same disorder? A fibroproliferative skin disorder hypothesis based on keloid findings. Int. Wound J. 11, 517–522.

Jacquet, E., Chambert, J., Pauchot, J., Sandoz, P., 2017a. Intra- and inter-individual variability in the mechanical properties of the human skin from in vivo measurements on 20 volunteers. Skin. Res. Technol. 23 (4), 491–499.

Jacquet, E., Joly, S., Chambert, J., Rekik, K., Sandoz, P., 2017b. Ultra-light extensometer for the assessment of the mechanical properties of the human skin in vivo. Skin. Res. Technol. 23 (4), 531–538.

Jemec, G., 2013. Dermatologic ultrasound with clinical and histologic correlations. Springer Science & Business Media.

Krusche, T., Worret, W.-I., 1995. Mechanical properties of keloids in vivo during treatment with intralesional triamcinolone acetonide. Arch. Dermatol. Res. 287, 289–293.

Lim, I. J., Phan, T.-T., Song, C., Tan, W., Longaker, M. T., 2001. Investigation of the influence of keloid-derived keratinocytes on fibroblast growth and proliferation in vitro. Plast. Reconstr. Surg. 107, 797–808.

Limandjaja, G. C., Broek, L. J., Waaijman, T., Veen, H. A., Everts, V., Monstrey, S., Scheper, R. J., Niessen, F. B., Gibbs, S., 2017. Increased epidermal thickness and abnormal epidermal differentiation in keloid scars. Br. J. Dermatol. 176, 116–126.

Marneros, A. G., Norris, J. E. C., Watanabe, S., Reichenberger, E., Olsen, B. R., 2004. Genome scans provide evidence for keloid susceptibility loci on chromosomes 2q23 and 7p11. J. Investig. Dermatol. 122, 1126–1132.

Meenakshi, J., Jayaraman, V., Ramakrishnan, K. M., Babu, M., 2005. Ultrastructural differentiation of abnormal scars. Ann. Burns Fire Disasters 18, 83.

Nagasao, T., Aramaki-Hattori, N., Shimizu, Y., Yoshitatsu, S., Takano, N., Kishi, K., 2013. Transformation of keloids is determined by stress occurrence patterns on perikeloid regions in response to body movement. Med. Hypotheses 81, 136–141.

Ogawa, R., 2008. Keloid and hypertrophic scarring may result from a mechanoreceptor or mechanosensitive nociceptor disorder. Med. Hypotheses 71, 493–500.

Ogawa, R., Hsu, C.-K., 2013. Mechanobiological dysregulation of the epidermis and dermis in skin disorders and in degeneration. J. Cell Mol. Med. 17, 817–822.

Ogawa, R., Okai, K., Tokumura, F., Mori, K., Ohmori, Y., Huang, C., Hyakusoku, H., Akaishi, S., 2012. The relationship between skin stretching/contraction and pathologic scarring: the important role of mechanical forces in keloid generation. Wound. Repair Regen. 20, 149–157.

Ogawa, R., Orgill, D. P., 2009. Mechanobiology of cutaneous wound healing and scarring. In: Bioengineering Research of Chronic Wounds. Springer, pp. 31–42.

O'Goshi, K.-I., 2006. Suction chamber method for measurement of skin mechanics: The Cutometer®. In: Serup, J., Jemec, G. B., Grove, G. L. (Eds.), Handbook of Non-Invasive Methods and the Skin, 2nd Edition. CRC Press, pp. 579–582.

Raghavan, M. L., Webster, M. W., Vorp, D. A., 1996. Ex vivo biomechanical behavior of abdominal aortic aneurysm: assessment using a new mathematical model. Ann. Biomed. Eng. 24, 573–582.

Ramakrishnan, K. M., Thomas, K. P., Sundararajan, C. R., 1974. Study of 1,000 patients with keloids in South India. Plast. Reconstr. Surg. 53, 276–280.

Reinholz, M., Schwaiger, H., Poetschke, J., Epple, A., Ruzicka, T., Von Braunmühl, T., Gauglitz, G. G., 2016. Objective and subjective treatment evaluation of scars using optical coherence tomography, sonography, photography, and standardised questionnaires. Eur. J. Dermatol. 26, 599–608.

Rockwell, W. B., Cohen, I. K., Ehrlich, H. P., 1989. Keloids and hypertrophic scars: A comprehensive review. Plast. Reconstr. Surg. 84, 827–837.

Salameh, F., Koren, A., Sprecher, E., Artzi, O., 2018. Novel stereoscopic optical system for objectively measuring above-surface scar volume—First-time quantification of responses to various treatment modalities. Dermatol. Surg. 44, 848–854.

Sattler, E. C., Kästle, R., Welzel, J., 2013. Optical coherence tomography in dermatology. J. Biomed. Opt. 18, 061224.

Schmitz, L., Reinhold, U., Bierhoff, E., Dirschka, T., 2013. Optical coherence tomography: its role in daily dermatological practice. J. Dtsch. Dermatol. Ges. 11, 499–507.

Suttho, D., Mankhetkorn, S., Binda, D., Pazart, L., Humbert, P., Rolin, G., 2017. 3D modeling of keloid scars in vitro by cell and tissue engineering. Arch. Dermatol. Res. 309, 55–62.

Ud-Din, S., Bayat, A., 2013. Strategic management of keloid disease in ethnic skin: a structured approach supported by the emerging literature. Br. J. Dermatol. 169, 71–81.

Wang, Z., Fong, K. D., Phan, T.-T., Lim, I. J., Longaker, M. T., Yang, G. P., 2006. Increased transcriptional response to mechanical strain in keloid fibroblasts due to increased focal adhesion complex formation. J. Cell. Physiol. 206, 510–517.

Wong, V. W., Akaishi, S., Longaker, M. T., Gurtner, G. C., 2011. Pushing back: wound mechanotransduction in repair and regeneration. J. Investig. Dermatol. 131, 2186–2196.

Wong, V. W., Beasley, B., Zepeda, J., Dauskardt, R. H., Yock, P. G., Longaker, M. T., Gurtner, G. C., 2013. A mechanomodulatory device to minimize incisional scar formation. Adv. Wound Care 2, 185–194.

Xu, F., Lu, T. J., Seffen, K. A., 2008. Biothermomechanical behavior of skin tissue. Acta Mech. Sin. 24, 1–23.